First-principles study of optical spectra of single-wall BC$_2$N nanotubes

Hui Pan,[1] Yuan Ping Feng,[1,*] and Jian Yi Lin[1,2]

[1]*Department of Physics, National University of Singapore, 2 Science Drive 2, Singapore 117542*
[2]*Institute of Chemical and Engineering Sciences, 1 Pesek Road, Jurong Island, Singapore 627833*
(Received 21 November 2005; published 13 January 2006)

First-principles calculations based on the density functional theory and the generalized gradient approximation were carried out to systematically investigate the optical properties of BC$_2$N nanotubes. Two types of zigzag nanotubes and two types of armchair nanotubes were considered. It was found that the optical properties of BC$_2$N nanotubes are closely related to their charility and diameter. Depending on the type of the nanotube, redshifts or blueshifts in the absorption peaks were observed which are due to the competition of the size effect and π orbital overlapping. Optical anisotropy with different light polarizations was also observed in the absorption spectra and loss function. The peaks in the loss function are attributed to the collective excitations of π electrons and the high-frequency $\pi+\sigma$ plasmon.

I. INTRODUCTION

Since its discovery, carbon nanotubes (CNT) have attracted ever increasing scientific interests. Besides the CNT, other compound nanotubes such as boron nitride (BN) nanotube have also been the focus of intensive theoretical and experimental studies, due to their potential applications.[1] Many works have been carried out to investigate the electronic and optical properties of carbon and BN nanotubes.[2–14]

The electronic properties of carbon nanotubes depend on their radii and chiralities.[15,16] Theoretical studies on optical and loss spectra of multiwall carbon nanotubes (MWCNTs) revealed a special structure at $\omega \sim 2\gamma_0$ ($\gamma_0 \sim 2.3-3.0$ eV is the nearest-neighbor overlap integral[17]) in the optical properties of MWCNTs.[18] For BN nanotubes, calculations showed that the energy gap of the zigzag nanotube decreases rapidly with the decrease in its radius, while that of the armchair BN nanotube remains almost constant.[19] It was shown that the strong electron-hole absorption peak of single-wall BN nanotubes at $\omega < 4\gamma_0$ comes from the π band and the other peaks above $4\gamma_0$ from the $\pi+\sigma$ bands.[11]

Recently, B$_x$C$_y$N$_z$ nanotubes, with arbitrary x, y, and z values, have been synthesized.[20,21] An important member of the family BC$_2$N has been studied and its electronic and elastic properties have been investigated.[22,23] In this paper, we present a first-principles study on the optical properties of the BC$_2$N nanotubes. Optical characterization is an important technique for understanding the physical properties of nanostructures. The aim of the study is to find a mapping between the electronic and optical properties of nanotubes and their structural properties.

II. CALCULATION DETAILS

First-principles method based on the density functional theory (DFT) (Ref. 24) and the generalized gradient approximation (GGA) (Ref. 25) were used in our study to investigate the optical properties of single-wall achiral BC$_2$N nanotubes. In our total-energy calculations, we used the plane-wave basis DFT pseudopotential method[24] and the CASTEP

code.[26] The ionic potentials were described by the ultrasoft pseudopotential proposed by Vanderbilt.[27] The Monkhorst and Pack scheme of k-point sampling was used for integration over the first Brillouin zone.[28] The Kohn-Sham energy functional is directly minimized using the conjugate-gradient method.[29] An energy cut-off of 310 eV and 10 k points along the axis of the tube in the reciprocal space were used in our calculation. Good convergence was obtained with these parameters and the total energy was converged to 2.0 $\times 10^{-5}$ eV/atom. A large supercell dimension in the plane perpendicular to the tube axis was used to avoid interaction between the BC$_2$N nanotube and its images in neighboring cells. The unit is periodic in the direction of the tube.

The imaginary part of the dielectric constant was calculated from the self-consistent electron wave-function Ψ_k and energy E_k,

$$\varepsilon_2(q \rightarrow O_{\hat{u}}, \hbar\omega) = \frac{2e^2\pi}{\Omega\varepsilon_0} \sum_{k,v,c} |\langle \Psi_k^c|\hat{u}\cdot r|\Psi_k^v\rangle|^2 \delta(E_k^c - E_k^v - E),$$

(1)

where $\hat{u}$ is a unit vector indicates the direction of the electric field of the incident light. The superscript $v(c)$ in Ψ_k and E_k labels the valence bands (conduction bands). Equation (1) is similar to the Fermi's golden rule for time dependent perturbation, and $\varepsilon_2(\omega)$ corresponds to real transitions between occupied and unoccupied electronic states. The real part $\varepsilon_1(\omega)$ of the dielectric constant was obtained from $\varepsilon_2(\omega)$ by using the Kramers-Kronig relation. A Gaussian smearing width of 0.5 eV was used in the calculation of the dielectric function.

III. RESULTS AND DISCUSSION

A. Structures of BC$_2$N nanotubes

A number of possible structures for planner BC$_2$N were considered. Our first-principles total-energy calculations showed that the geometry given in Fig. 1 is most stable, which is consistent with previous reported results.[22,30] The covalent bond lengths in the fully optimized structures are
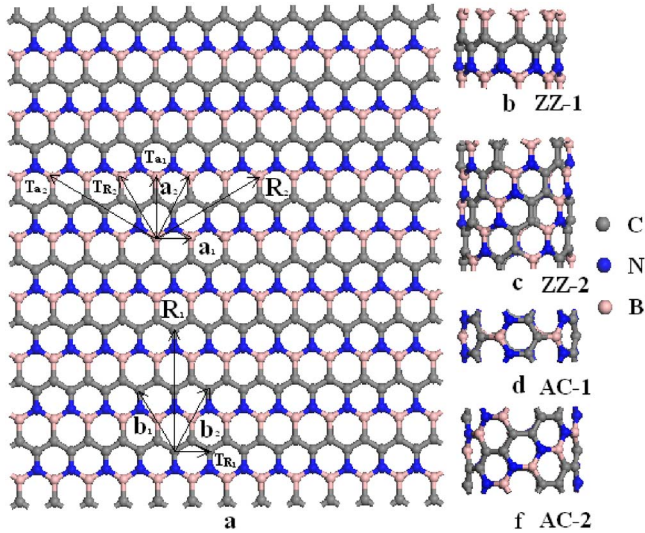
FIG. 1. (Color online) Atomic configuration of an isolated BC_2N sheet. Primitive and translational vectors are indicated.

FIG. 2. Absorption spectra of AC-1 (n,n): (a) for parallel light polarization and (b) for perpendicular light polarization. The curves are displaced vertically for clarity (also applies to other figures).

given in Table I. These and other structure details are in good agreement with those of Refs. 22 and 30.

As shown in Fig. 1, there are several ways of rolling up the BC_2N sheet into zigzag, or armchair nanotubes compared to a carbon sheet because of its anisotropic geometry. If the vector notation of carbon nanotubes[31] is followed, two kinds of zigzag BC_2N nanotubes, along a_1 and a_2, respectively, and two kinds of armchair nanotubes, along R_1 and R_2, respectively, can be obtained. To investigate the chiral dependence of the optical properties of BC_2N nanotubes, all four types of nanotubes were considered. For convenience, they are referred to as ZZ-1 for the zigzag tube obtained by rolling up the BC_2N sheet along a_1, ZZ-2 for the zigzag tube rolled up along a_2, AC-1 for the armchair tube rolled up along R_1, and AC-2 for the armchair tube rolled up along R_2, respectively. The corresponding translational lattice vectors along the tube axes, T_{a1}, T_{a2}, T_{R1}, and T_{R2}, respectively, are shown in Fig. 1. To investigate diameter dependence of optical properties of the BC_2N nanotubes, different sizes of each type of tubes, ZZ-1 $(n,0)$ for $n=6,\ldots,20$, ZZ-2 $(0,n)$, AC-1 (n,n), and AC-2 (n,n), with $n=2-5$, were considered. Structures of all nanotubes were fully optimized. The bond lengths in the optimized structures are slightly deviated from those in the planner BC_2N structure (See Table I). The calculated band gaps and structures are size- and chirality-dependent. With the increase in the tube size, the band gap

TABLE I. Bond length in the fully optimized planner BC_2N structure and BC_2N nanotube.

Bond	Length (Å)	
	BC_2N sheet	BC_2N tube
C-C	1.42	1.42
C-B	1.56	1.51
C-N	1.32	1.39
B-N	1.43	1.45

converges to 1.61 eV which is underestimated due to the well known problem with GGA.

B. Chirality and size dependence of absorption spectra

Figure 2 shows the absorption spectra of AC-1 type BC_2N nanotubes of different diameters. First of all, optical anisotropy can be clearly seen. The absorption spectra under parallel and perpendicular light polarizations show clearly different features. For parallel light polarization, the first peak is at ~ 3.1 eV [Fig. 2(a)], which is mainly attributed to the inter-π band transitions. This low-energy absorption peak was not observed in the absorption spectra of boron nitride nanotubes,[12] but was present in the absorption spectra of carbon nanotubes.[13] With the increase of the tube diameter (or n from 2–5), the peak is slightly blueshifted (from 2.94 to 3.31 eV). The π band to π^* band transition at ~ 7.5 eV is also blueshifted from 7.11 to 7.71 eV when the diameter of the tube increases, i.e., n increases from 2–5. The peaks above 10.0 eV are enhanced in larger tubes, especially the peak around 18.0 eV. The position of the peak around 14.8 eV remains the same with the change of tube size. But the peaks around 18.0 and 21.8 eV slightly redshift with the increase of the tube size. The peaks above 10.0 eV are attributed to the inter-σ band transitions. The range of the σ band transition is wider than that of the π band transition. The situation is different for the perpendicular light polarization [Fig. 2(b)]. Here the first absorption peak is around 1.5 eV and it redshifts from 1.66 to 1.16 eV with the increase of the tube diameter (n from 2–5). There exists another weak peak around 5.2 eV which gains strength and redshifts with an increasing tube diameter. The broad σ band transitions above 10.0 eV redshift with increasing tube diameter.

The absorption spectra of the AC-2 type nanotubes are shown in Fig. 3. For light polarization parallel to the tube axis, the main absorption peak is located near 14.5 eV [Fig. 3(a)]. As the diameter of the tube increases, i.e., n increases from 2–5, this pronounced σ band absorption peak redshifts from 14.64 to 14.32 eV. There exist other peaks in the low-energy wavelength. The π band transition around 2.3 eV is
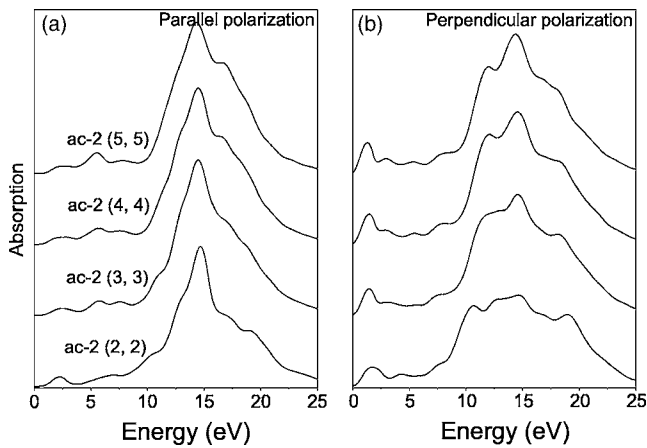
FIG. 3. Absorption spectra of AC-2 (m,m): (a) for parallel light polarization and (b) for perpendicular light polarization.

blueshifts, suppressed with increasing tube diameter and almost disappears in AC-2 (5, 5). The π band transition around 5.5 eV redshifts and gains strength as the diameter of the tube increases. Compared to the AC-1 tube, only one dominant peak for the σ band transition exists in the parallel polarization absorption spectrum of AC-2. In the case of perpendicular light polarization, the main absorption peak is located around 14.6 eV and is slightly redshifted from 14.69 to 14.43 eV when n increases from 2–5 [Fig. 3(b)]. A nearby peak, around 12.5 eV, gains strength and redshifts from 12.76 to 11.94 eV as n varies from 2–5. The peak around 1.5 eV corresponds to the π band transition. It is slightly redshifted.

Figure 4 shows the absorption spectra of the ZZ-1 type BC_2N nanotubes. For light polarization parallel to the tube axis, the main absorption peaks are within the range of 10.0 to 20.0 eV, corresponding to σ band transitions. Two of the peaks are prominent and shift in opposite directions with
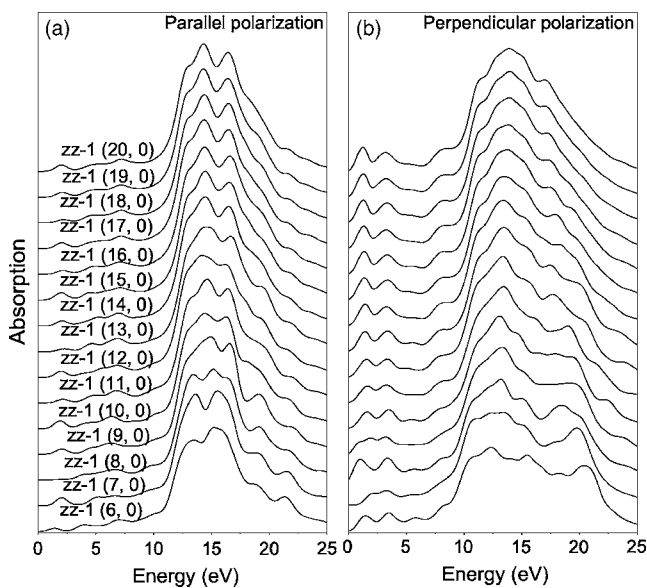
FIG. 4. Absorption spectra of ZZ-1 $(n,0)$: (a) for parallel light polarization and (b) for perpendicular light polarization.
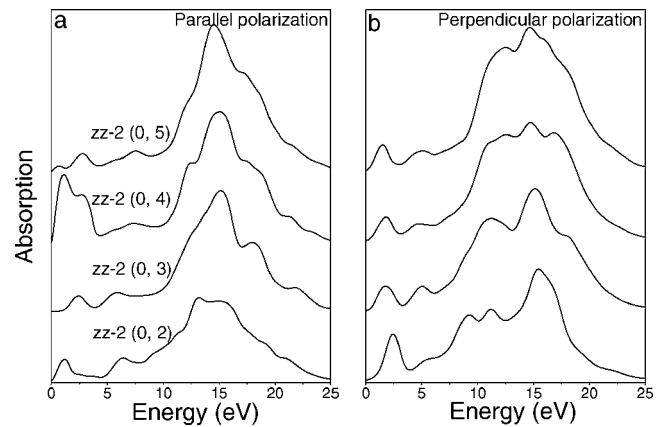
FIG. 5. Absorption spectra of ZZ-2 $(0,n)$: (a) for parallel light polarization and (b) for perpendicular light polarization.

increasing tube size. The peak around 14.5 eV redshifts from 14.83 to 14.25 eV when n increases from 12–20. The peak around 16.5 eV blueshifts from 16.35 to 16.55 eV when n increases from 13–20 [Fig. 4(a)]. The shoulderlike structures on both sides of the above peaks suggest existence of two weak peaks, the one at higher energy redshifts and is suppressed, but the one at lower energy essentially remains where it is as the size of the tube increases. Absorption peaks are also observed in the low-energy range. The peak around 2.0 eV remains at the same energy, but the peak at 7.0 eV is blueshifted from 6.32 to 7.24 eV with n increasing from 8–20. Several absorption peaks are observed in the case of perpendicular light polarization. The first absorption peak redshifts from 1.53 to 1.18 eV with n increasing from 10–20 [Fig. 4(b)]. The peak around 3.3 eV redshifts slightly and becomes more intense with the increase of the tube size. The σ band transitions above 9.7 eV blueshifts to certain degrees, and one of them vanishes gradually with increasing tube diameter.

For the ZZ-2 type BC_2N nanotubes (Fig. 5), the pronounced absorption corresponding to the σ band transitions is broad and centers around 15.0 eV, which redshifts from 15.56 to 14.58 eV as the diameter of the tube increases in the case of parallel light polarization [Fig. 5(a)]. The π band transition below 5.0 eV for ZZ-2 (0, 4) is broad and different from that of ZZ-2 $(0,n)$ $(n \neq 4)$. For light polarization perpendicular to the tube axis, the σ band transitions center around 15.0 eV, which redshifts from 15.44 to 14.71 eV as the diameter of the tube increases in the case of parallel light polarization [Fig. 5(b)]. The first π band transition around 2.0 eV redshifts from 2.45 to 1.47 eV as the tube diameter increases. No noticeable shift was found for the second π band transition around 5.0 eV.

The absorption spectra of the four series of BC_2N nanotubes given above show clear optical anisotropy with respect to light polarization. This can be attributed to the local field effect due to depolarization. It is also shown that the absorption spectra are chirality and size dependent. For a given chirality, redshifts or blueshifts in the position of the absorption peak is possible with an increase in the tube diameter, which is due to the competition between the size effect and π orbitals overlapping.[32] The optical gap will eventually satu-
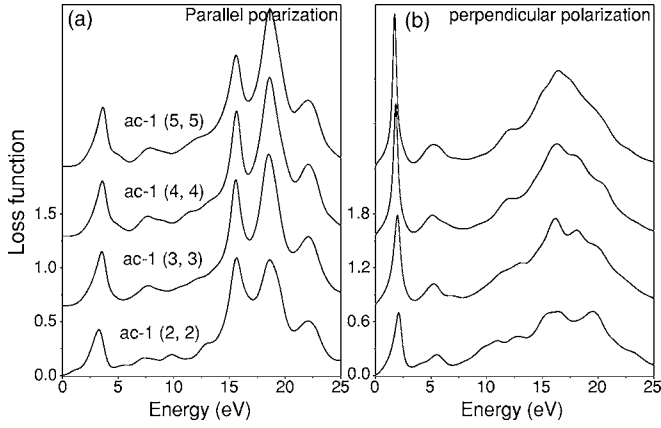
FIG. 6. Loss functions of AC-1 (n,n): (a) for parallel light polarization and (b) for perpendicular light polarization.

FIG. 7. Loss functions of AC-2 (m,m): (a) for parallel light polarization and (b) for perpendicular light polarization.

rate when the tube diameter reaches a certain value, due to the reduction of curvature induced hybridization effect.[33] It is noted that the first absorption peak, which should correspond to the optical gap, is above 2.5 eV and is larger than the calculated energy gap (about 1.6 eV).

C. Chirality and size dependence of loss function

The loss function is a direct probe of collective excitation of the system under consideration. We have calculated the loss functions of the BC_2N nanotubes using $Im(-1/\varepsilon(\omega))$ at zero momentum transfer from the macroscopic dielectric function $\varepsilon(\omega)=\varepsilon_1(\omega)+i\varepsilon_2(\omega)$. The calculated loss functions of the AC-1 type BC_2N nanotubes are shown in Fig. 6. Several peaks are observed, which are related to the one-dimensional (1D) subbands with divergent density of states. Under parallel light polarization, the first peak in the loss function is around 3.5 eV [Fig. 6(a)], which can be attributed to the inter-π transition. The peak blueshifts from 3.25 to 3.64 eV with the increase of the tube diameter. Another peak is located around 7.5 eV which is contributed to the collective excitation π electrons and becomes apparent with increasing tube diameters. Three peaks above 12.0 eV are contributed to $\pi+\sigma$ plasmon.[8] And the peak at 18.6 eV gains strength with the increase of the tube size. In the case of perpendicular polarization, the main peak is around 2.0 eV which is attributed to the interband transition[18] and shifts from 2.12 to 1.72 eV as the tube diameter increases [Fig. 6(b)]. The peak around 5.3 eV is due to the collective excitation of π electrons. Peaks are also observed above 10.0 eV, which are attributed to the higher-frequency $\pi+\sigma$ plasmon.[8] Generally, the higher-frequency $\pi+\sigma$ plasmon is stronger than the collective excitation π electrons because the density of $\pi+\sigma$ electrons is larger than that of π electrons.

Figure 7 shows the loss functions of the AC-2 type BC_2N nanotubes under different polarizations. In the case of parallel polarization, the inter-π transition redshifts slightly from 2.38 to 2.27 eV with the strength suppressed as the diameter of the tube increases [Fig. 7(a)]. The collective excitation of π electrons around 5.8 eV remains there and gains strength as the diameter of the tube increases. High-frequency $\pi+\sigma$
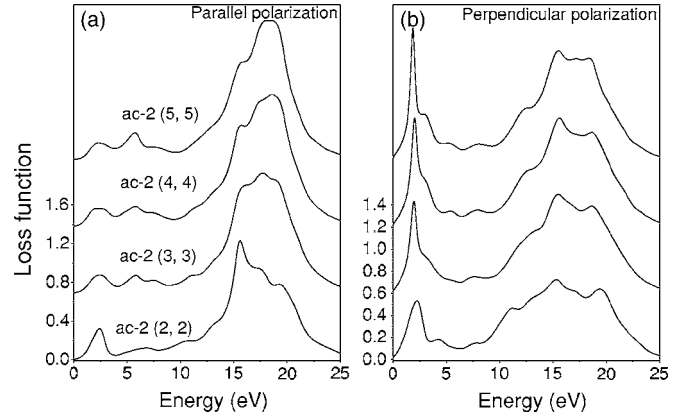
plasma is in the range of 12.0 to 22.0 eV and its peak slightly blueshifts as the diameter of the tube increases. For perpendicular polarization, the weak π plasma excitation occurs around 7.5 eV [Fig. 7(b)]. The interband transition peak located around 2.0 eV shifts from 2.18 to 1.85 eV with the increase of the tube diameter. High-frequency $\pi+\sigma$ plasma with broad band excitation are also observed above 10.0 eV.

The loss functions of the ZZ-1 type BC_2N nanotubes under parallel light polarization are showed in Fig. 8(a). The inter-π transition redshifts slightly from 2.28 to 2.17 eV as n increases from 7–20. The weak collective excitation of π electrons is located around 7.1 eV and blueshifts slightly as the diameter of the tube increases. High-frequency $\pi+\sigma$ plasma is in the range 12.0–22.0 eV and its peak slightly blueshifts as the diameter of the tube increases. For perpendicular polarization, the weak π plasma excitation occurs around 8.2 eV [Fig. 8(b)]. The interband transition peaks are located within the range 0–5 eV. The lower-energy interband transition around 1.7 eV gains strength with the increase of the tube diameter. High-frequency $\pi+\sigma$ plasma
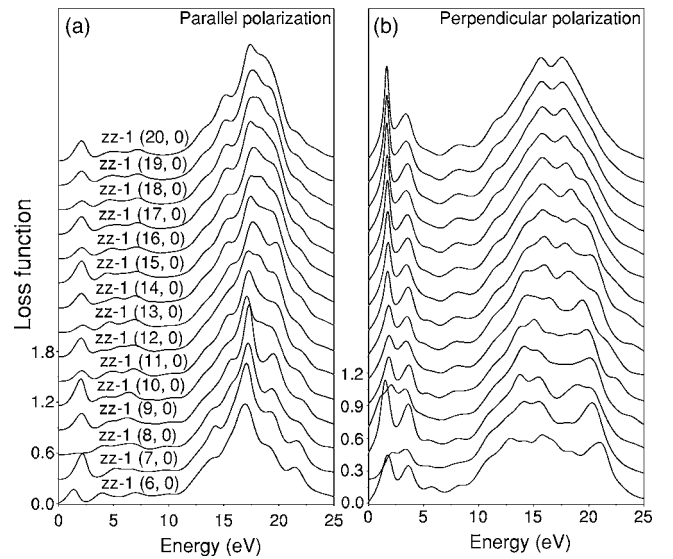
FIG. 8. Loss functions of ZZ-1 $(n,0)$: (a) for parallel light polarization and (b) for perpendicular light polarization.
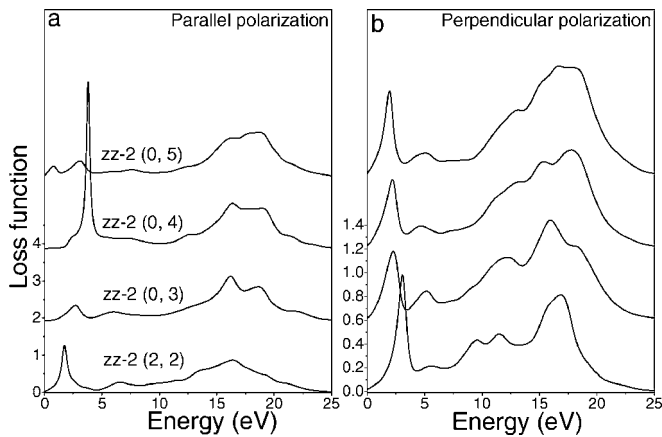
FIG. 9. Loss functions of ZZ-2 $(0,n)$: (a) for parallel light polarization and (b) for perpendicular light polarization.

with broad band excitation are also observed above 10.0 eV. Two excitation peaks remain prominent as the diameter increases.

The loss functions of the ZZ-2 type BC_2N nanotubes are shown in Fig. 9. For parallel polarization, the $\pi+\sigma$ plasma is in the range 12.0–20.0 eV and blueshift with the increase in the diameter of the tube [Fig. 9(a)]. The inter-π-band transition around 3.7 eV is very strong for ZZ-2 (0, 4). The weak π plasma around 7.0 eV blueshifts as the tube diameter increases. Under perpendicular polarization, the the $\pi+\sigma$ plasma is within 9.0–20.0 eV [Fig. 9(b)] and blueshifts as the tube diameter increases. The inter-π-band transition around 2.0 eV redshifts from 3.06 to 1.89 eV as the tube diameter increases. The π plasma around 5.0 eV redshifts slightly as the tube diameter increases.

From the above, we can see that the loss functions of the BC_2N nanotubes have anisotropy in the plasma excitation with different light polarizations. Generally, the inter-π-band excitation energy is less than 5.0 eV. The π plasmon excitation energy is within the range 5.0 eV–9.0 eV. The high-frequency $\pi+\sigma$ plasmon is observable above 10.0 eV. The intensity of the π plasma is much weaker than that of $\pi+\sigma$ plasma because the density of $\pi+\sigma$ electrons is larger than that of π electrons. The peaks shift slightly with the increase of the tube diameter.

IV. CONCLUSIONS

In summary, we systematically studied the optical properties of BC_2N nanotubes using a first-principles method. It was found that the absorption spectra and loss functions of the BC_2N nanotubes are closely related to their diameter and charility. Optical anisotropy is observed for different light polarizations. The absorption spectra indicate that the optical gap can redshift or blueshift with the increase in the tube diameter, depending on the charility. The observation of low-energy absorption in BC_2N nanotubes indicate that BC_2N nanotubes have similar optical properties as carbon nanotubes to some extent due to their similar π bonding consisting of carbon p orbitals. The pronounced peaks in the loss function spectra are mainly induced by the collective excitation of π electrons below 10.0 eV and the high-frequency $\pi+\sigma$ plasmon above 10.0 eV. The collective excitation of π electrons is much weaker than that of the high-frequency $\pi+\sigma$ plasmon. It is noted that due to the well known fact that DFT/GGA underestimates band gaps of semiconductors, a systematic shift for the peak positions may be necessary in the calculated optical spectra. However, the dependence of the optical properties of BC_2N naotubes on their size and charility are valid.

*Corresponding author; Email address: phyfyp@nus.edu.sg

[1] S. Iijima, Nature (London) **354**, 56 (1991).

[2] A. Rubio, J. L. Corkill, and M. L. Cohen, Phys. Rev. B **49**, 5081 (1994).

[3] P. Chen, X. Wu, X. Sun, J. Lin, W. Ji, and K. L. Tan, Phys. Rev. Lett. **82**, 2548 (1999).

[4] S. Reich, C. Thomsen, and P. Ordejon, Phys. Rev. B **65**, 155411 (2002).

[5] X.-P. Tang, A. Kleinhammes, H. Shimoda, L. Fleming, K. Y. Bennoune, S. Sinha, C. Bower, O. Zhou, and Y. Wu, Science **288**, 492 (2000).

[6] A. A. Maarouf, C. L. Kane, and E. J. Mele, Phys. Rev. B **61**, 11156 (2000).

[7] F. J. Garcia-Vidal, J. M. Pitarke, and J. B. Pendry, Phys. Rev. Lett. **78**, 4289 (1997).

[8] A. G. Marinopoulos, L. Reining, A. Rubio, and N. Vast, Phys. Rev. Lett. **91**, 046402 (2003).

[9] G. G. Fuentes, E. Borowiak-Palen, T. Pichler, X. Liu, A. Graff, G. Behr, R. J. Kalenczuk, M. Knupfer, and J. Fink, Phys. Rev. B **67**, 035429 (2003).

[10] H. J. Xiang, J. Yang, J. G. Hou, and Q. Zhu, Phys. Rev. B **68**, 035427 (2003).

[11] R. B. Chen, F. L. Shyu, C. P. Chang, and M. F. Lin, J. Phys. Soc. Jpn. **71**, 2286 (2002).

[12] M.-F. Ng and R. Q. Zhang, Phys. Rev. B **69**, 115417 (2004).

[13] M. F. Lin, Phys. Rev. B **62**, 13153 (2000).

[14] G. Y. Guo and J. C. Lin, Phys. Rev. B **71**, 165402 (2005).

[15] N. Hamada, S. I. Sawada, and A. Oshiyama, Phys. Rev. Lett. **68**, 1579 (1992).

[16] M. S. Dresselhaus, G. Dresselhaus, and R. Saito, Solid State Commun. **84**, 201 (1992).

[17] J. W. Mintmire, B. I. Dunlap, and C. T. White, Phys. Rev. Lett. **68**, 631 (1992).

[18] M. F. Lin, F. L. Shyu, and R. B. Chen, Phys. Rev. B **61**, 14114 (2000).

[19] H. J. Xiang, J. Yang, J. G. Hou, and Q. Zhu, Phys. Rev. B **68**, 035427 (2003).

[20] Z. Weng-Sieh, K. Cherrey, N. G. Chopra, X. Blase, Y. Miyamoto, A. Rubio, M. L. Cohen, S. G. Louie, A. Zettl, and R. Gronsky, Phys. Rev. B **51**, 11229 (1995).

[21] K. Suenaga, C. Colliex, N. Demoncy, A. Loiseau, H. Pascard, and F. Willaime, Science **278**, 653 (1997).

[22] Y. Miyamoto, A. Rubio, M. L. Cohen, and S. G. Louie, Phys. Rev. B **50**, 4976 (1994).

[23] E. Hernández, C. Goze, P. Bernier, and A. Rubio, Phys. Rev. Lett. **80**, 4502 (1998).

[24] M. C. Payne, M. P. Teter, and D. C. Allan, Rev. Mod. Phys. **64**, 1045 (1992).

[25] J. P. Perdew and Y. Wang, Phys. Rev. B **45**, 13244 (1992).

[26] M. D. Segall, P. J. D. Lindan, M. J. Probert, C. J. Pickard, P. J. Hasnip, S. J. Clark, and M. C. Payne, J. Phys.: Condens. Matter **14**, 2717 (2002).

[27] D. Vanderbilt, Phys. Rev. B **41**, R7892 (1990).

[28] H. J. Monkhorst and J. Pack, Phys. Rev. B **13**, 5188 (1976).

[29] M. P. Teter, M. C. Payne, and D. C. Allan, Phys. Rev. B **40**, 12255 (1989).

[30] A. Y. Liu, R. M. Wentzcovitch, and M. L. Cohen, Phys. Rev. B **39**, 1760 (1989).

[31] M. S. Dresselhaus, G. Dresslhaus, and P. C. Eklund, *Science of Fullerenes and Carbon Nanotubes* (Acadamic Press, San Diego, 1996), p. 804.

[32] W. Z. Liang, X. J. Wang, S. Yokojima, and G. H. Chen, J. Am. Chem. Soc. **122**, 11129 (2000).

[33] A. Zunger, A. Katzir, and A. Halperin, Phys. Rev. B **13**, 5560 (1974).